Probing Magnetic Excitations in a Co(II) Single-Molecule Magnet by Inelastic Neutron Scattering

Shelby E. Stavretis,[a] Yongqiang Cheng,[b,*] Luke L. Daemen,[b,*] Craig M. Brown,[c,d,*] Duncan H. Moseley,[a] Eckhard Bill,[e,*] Mihail Atanasov,[f,g] Anibal J. Ramirez-Cuesta,[b] Frank Neese,[f] Zi-Ling Xue[a,*]

[a] Shelby E. Stavretis, Duncan H. Moseley, Prof. Zi-Ling Xue, *Department of Chemistry, University of Tennessee, Knoxville, Tennessee 37996, USA*; Email: xue@ion.chem.utk.edu; Web: https://xue.utk.edu/

[b] Dr. Yongqiang Cheng, Dr. Luke L. Daemen, Dr. Anibal J. Ramirez-Cuesta *Neutron Scattering Division, Oak Ridge National Laboratory, Oak Ridge, Tennessee 37831, USA;* Emails: chengy@ornl.gov; daemenll@ornl.gov; Webs: https://neutrons.ornl.gov/contacts/chengy; https://neutrons.ornl.gov/contacts/daemenll;

[c] Dr. Craig M. Brown, *NIST Center for Neutron Research, National Institute of Standards and Technology, Gaithersburg, Maryland 20899, USA*

Email: craig.brown@nist.gov; Web: https://www.ncnr.nist.gov/staff/craig/index.html

[d] *Department of Chemical and Biomolecular Engineering, University of Delaware, Newark, Delaware 19716, USA*

[e] Dr. Eckhard Bill, *Max Planck Institute for Chemical Energy Conversion, Stiftstraße 34-36, D-45470, Mülheim an der Ruhr, Germany*; Email: eckhard.bill@cec.mpg.de; Web: https://cec.mpg.de/en/research/molecular-theory-and-spectroscopy/dr-eckhard-bill/

[f] Prof. Dr. Mihail Atanasov; Prof. Dr. Frank Neese, *Max Planck Institute for Coal Research, Kaiser-Wilhelm-Platz 1, D-45470 Mülheim an der Ruhr, Germany*

[g] *Institute of General and Inorganic Chemistry, Bulgarian Academy of Sciences, 1113 Sofia, Bulgaria*

Abstract

$Co(acac)_2(H_2O)_2$ (**1**, acac = acetylacetonate), a transition metal complex (S = 3/2), displays field-induced slow magnetic relaxation as a single-molecule magnet. For **1** and its isotopologues $Co(acac)_2(D_2O)_2$ (**1-*d*$_4$**) and $Co(acac\text{-}d_7)_2(D_2O)_2$ (**1-*d*$_{18}$**) in appropriately D_{4h} symmetry, zero-field splitting of the ground electronic state leads to two Kramers doublets (KDs): lower energy $M_S = \pm 1/2$ ($\phi_{1,2}$) and higher energy $M_S = \pm 3/2$ ($\phi_{3,4}$) states. Inelastic neutron scattering (INS), a unique method to probe magnetic transitions, has been used to probe different magnetic excitations in **1-*d*$_4$** and **1-*d*$_{18}$**. The direct-geometry, time-of-flight Disk-Chopper Spectrometer (DCS), with applied magnetic fields up to 10 T, has been used to study the intra-KD transition as a result of Zeeman splitting, $M_S = -1/2$ (ϕ_1) $\rightarrow$ $M_S = +1/2$ (ϕ_2), in **1-*d*$_{18}$**. This is a rare study of the $M_S = -1/2 \rightarrow M_S = +1/2$ excitation in transition metal complexes by INS. The indirect-geometry INS spectrometer VISION has been used to probe the inter-KD, ZFS transition, $M_S = \pm 1/2$ ($\phi_{1,2}$) $\rightarrow$ $M_S = \pm 3/2$ ($\phi_{3,4}$) in both **1-*d*$_4$** and **1-*d*$_{18}$**. Variable-temperature (VT) properties of this excitation near 114 cm^{-1} have been used to identify the ZFS transition. The INS spectra measured on VISION also give phonon features of the complexes that are well described by *ab initio* phonon calculations.

Introduction

Determination of magnetic excitations is vital for the detection and understanding of the origin of the magnetic anisotropy of metal complexes including single-molecule magnets (SMMs).[1] There exist many challenges in identifying large magnetic excitations (>33 cm^{-1}) with spectroscopic methods. This is mainly because there are few techniques to directly observe such large magnetic excitations, and phonons of the compounds are prevalent in the range, which overlap with the magnetic peaks making the identification of magnetic peaks difficult. Inelastic neutron scattering (INS) is a unique, direct probe[2] to study magnetic excitations in complexes of both d-[2b, 3] and f-elements.[4] In INS, magnetic excitations can be determined by a variety of methods: (1) Temperature dependence; (2) $|\boldsymbol{Q}|$ dependence; (3) Diamagnetic control; (4) Application of an external magnetic field. One challenge that is relevant solely to INS is the strong incoherent scattering from H atoms in ligands of metal complexes. The use of temperature dependence and diamagnetic controls has been previously utilized as a method to distinguish magnetic excitations in INS. For example, deuterated carbonate-bridged lanthanide (Ho^{III} and Er^{III}) triangles were synthesized along with the diamagnetic Y^{III} analogue (for comparison of phonon background) to find the magnetic excitation with variable temperatures.[4a] These excitations were found at 24-80 cm^{-1} (3-10 meV).

Characterization of phonons of magnetic complexes such as SMMs is important to understanding spin-phonon coupling and magnetic relaxation of the SMMs.[5] INS is a well-established technique to probe phonons in molecular solids in comparison with optical methods such as IR and Raman.[6] Unique features of INS include: (a) There are no symmetry selection rules for INS; (b) Scattering of H atoms is prominent relative to

other atoms; (c) INS spectra can be more easily calculated.

Magnetic and phonon peaks exhibit different temperature dependences. The Bose correction has been used to distingusih the magnetic excitation in INS.[2b] The correction applies a frequency- and temperature-dependent normalization factor such that INS spectra measured at different temperatures are brought to a similar level for easy comparison. For pure phonons following Bose-Einstein statistics, the normalized spectra are expected to have similar profile and baseline intensity. In other words, the normalization highlights features that do not follow the expected temperature dependence for pure phonons, which in turn suggests possible magnetic or mixed origin. A peak at ~95.2 cm^{-1} in the INS spectra of a Co^{II}-Y^{III} dinuclear SMM, for example, was determined to show the greatest intensity drop between 4 and 100 K and therefore assigned to be a magnetic excitation.[2b]

$Co(acac)_2(H_2O)_2$ (**1**; Figure 1; S = 3/2 SMM; $2D' = 2(D^2 + 3E^2)^{1/2} \approx 114$ cm^{-1}; D and E = axial and rhombic zero-field splitting (ZFS) parameters, respectively; $D > 0$)[7] and its isotopologues $Co(acac)_2(D_2O)_2$ (**1-*d*$_4$**) and $Co(acac\text{-}d_7)_2(D_2O)_2$ (**1-*d*$_{18}$**)[7-8] have been studied by magnetometry and spectroscopies. We have recently found spin-phonon coupling between the inter-Kramers doublet (inter-KD or ZFS) magnetic transition and nearby phonons in **1**, **1-*d*$_4$** and **1-*d*$_{18}$** by far-IR and Raman spectroscopies inside magnetic fields.[8a] The current work details our studies of two magnetic transitions by INS: (1) M_S = -1/2 (ϕ_1) $\rightarrow$ M_S = +1/2 (ϕ_2) in **1-*d*$_{18}$** and confirmation of the sign of D by direct-geometry INS with an external magnet; (2) $M_S = \pm 1/2$ ($\phi_{1,2}$) $\rightarrow$ $M_S = \pm 3/2$ ($\phi_{3,4}$) transitions in both **1-*d*$_4$** and **1-*d*$_{18}$** by indirect-geometry INS without an external magnet. Since the complex is highly rhombic, all the transitions should be in

principle INS allowed, although at 1.7 K the transitions are most likely from the ground state M_S = -1/2 (ϕ_1).[8a, 9] INS with magnetic fields to probe molecular magnetism has rarely been used.[10] Although we observed the inter-KD (ZFS) transition by far-IR and Raman under magnetic fields,[8a] here we report in the complementary INS spectra of the transition without an external magnet to see how VT features of the INS lead to the identification of the magnetic transition. The studies by an indirect-geometry INS spectrometer also give phonon features of the complexes. Earlier, results of periodic DFT phonon calculations for the 70-160 cm^{-1} region of **1-*d*$_4$** and **1-*d*$_{18}$** (near the inter-KD transition at 114 cm^{-1}) were presented.[8a] In addition, INS spectra of the 15-250 cm^{-1} region at 5 and 100 K for **1-*d*$_4$** recorded at VISION (without magnet) were given to show the methyl torsion peak in the complex.[8b] The spectra in this limited region were used to understand the effect of magnetic fields on the methyl rotation in quasielastic neutron scattering (QENS) spectra. Here, we present the following INS spectra: (a) Variable-magnetic-field INS (0-25 cm^{-1}) of **1-*d*$_{18}$** at DCS (0-10 T); (b) VT INS (0-4000 cm^{-1}) of **1-*d*$_{18}$** at VISION (5, 25, 50, 100 and 150 K); (c) VT INS (0-4000 cm^{-1}) of **1-*d*$_4$** at VISION (5, 50, 100 and 150 K). The calculated phonons for the entire 0-4000 cm^{-1} region are reported here in order to compare with the experimental INS spectra in the current work.

Results and Discussion

The high-spin, d^7 hexacoordinated Co(II) complex **1** (Figure 1a) shows local symmetry approximated to D_{2h} with the ground electronic state of $^4A_{2g}$.[7] For $D > 0$ and $E/D \approx 0$, d metal complexes in tetragonal environments such as D_{4h}, zero-field splitting (ZFS) leads to two Kramers doublets (KDs): ground state $M_S = \pm 1/2$ and excited state

M_S = ±3/2. In non-tetragonal environments, rhombicity ($E/D \neq 0$) and mixing of the states occur, giving four mixed states noted in Figure 1b.[8a] Although, after the mixing, describing the two KDs as M_S = ±1/2 and ±3/2 is not precise anymore, these labels are used here for simplicity. Inside magnetic fields, each KD splits by the Zeeman effect (Figure 1c). The two transitions probed by INS in the current work are indicated by the blue arrows in Figure 1.

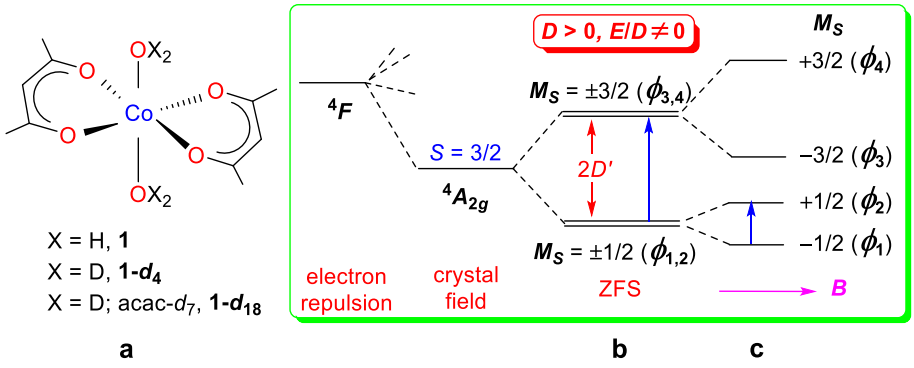

Figure 1. (a) Structures of **1**, **1-*d*$_4$** and **1-*d*$_{18}$**. (b) Ground-state quartet levels in high-spin, d^7 complexes with D_{4h} symmetry and $D > 0$; $D' = (D^2 + 3E^2)^{1/2}$; The quartet levels in **1** with lower symmetry: $\phi_1 = -a\,|-1/2\rangle + b\,|+3/2\rangle$; $\phi_2 = a\,|+1/2\rangle - b\,|-3/2\rangle$; $\phi_3 = b\,|+1/2\rangle + a\,|-3/2\rangle$; $\phi_4 = b\,|-1/2\rangle + a\,|+3/2\rangle$ where the mixing coefficients a = cos β; b = sin β; tan 2β = √3 (E/D) (SI of Ref. 7). (c) Zeeman splitting of the Kramers doublets inside magnetic field ***B***.

Direct- and Indirect-Geometry Spectrometers for the Current INS Studies

There are two types of time-of-flight (TOF) instruments for INS, direct- and indirect-geometry spectrometers (Scheme 1). Disk Chopper Spectrometer (DCS,[11] NIST National Center for Neutron Research, Gaithersburg, MD) is an example of direct

geometry instruments in the United States. The Vibrational Spectrometer (VISION,[12] ORNL) is an example of an indirect-geometry instrument. Each type of the spectrometers has advantages and disadvantages as summarized below.

A direct-geometry spectrometer has a fixed incident neutron energy E_i and the energy transfer between the neutrons and the sample is obtained by measuring scattered intensity as a function of E_f (Scheme 1, top-left) so as to measure the energy transferred to and from the sample, $\hbar\omega = E_i - E_f$.[2a] In the case of DCS, E_i is defined by a series of choppers that select a single energy from an incident white beam and pulses it, with E_f measured by time-of-flight (TOF) of the neutrons.[13] There is a large detector array at different scattering angles enabling a wide range of momentum transfer ($\boldsymbol{Q}$), and energy transfer ($\hbar\omega$) to be measured. DCS is also flexible in the choice of incident energy, and has two resolution modes that can be used to maintain the $|\boldsymbol{Q}|$-range, while reducing the resolution by a factor of two, at the cost of a loss of about a factor in 8 in intensity. The range in neutron-energy gain is large (ca. 200 cm^{-1}), but practically depends on the populations of higher level states above the ground state from which the neutron can gain energy. The resolution on this side of the spectrum gets worse with increasing energy transfer. The range in neutron energy loss, is essentially determined by E_i and the resolution on this side of the elastic line improves with increasing energy transfer. For the low resolution, high flux setting of E_i = 200 cm^{-1}, the elastic line resolution 16 cm^{-1} improves to 8 cm^{-1} by E_i = 160 cm^{-1}. With this setting, the $|\boldsymbol{Q}|$-range is 0.3-6.5 $Å^{-1}$ allowing access to small $|\boldsymbol{Q}|$, where the magnetic form-factor results in maximum signal intensities. Direct geometry instruments can easily be paired with an external magnetic field in the sample environment. For example, DCS can reach

fields up to 11.5 T.

In the current studies, approximately 2 g of **1-d_{18}** placed in an aluminum sample holder at 1.7 K were used for variable-magnetic-field INS studies at DCS with a 10-T vertical magnet. Two studies were performed: (a) Incident neutron energy of 32.6 cm^{-1} (wavelength = 4.5 Å) to observe the intra-KD_1 ["M_S = -1/2 (ϕ_1) $\rightarrow$ +1/2"] transition at 0, 2, 4, 6, 8 and 10 T. Results are discussed below. (b) Incident energy of 203.6 cm^{-1} (wavelength = 1.8 Å) at 0 and 10 T to observe the inter-KD ["M_S = $\pm$1/2 ($\phi_{1,2}$) $\rightarrow$ $\pm$3/2 ($\phi_{3,4}$)" at 0 T and "M_S = -1/2 (ϕ_1) $\rightarrow$ +3/2 (ϕ_4)" at 10 T[8a]] transitions. There is some evidence that the transitions at and near 114 cm^{-1} is observable from DCS data as a function of field, but the signal/noise ratio prevents a conclusive assignment. These data are in the SI for completeness.

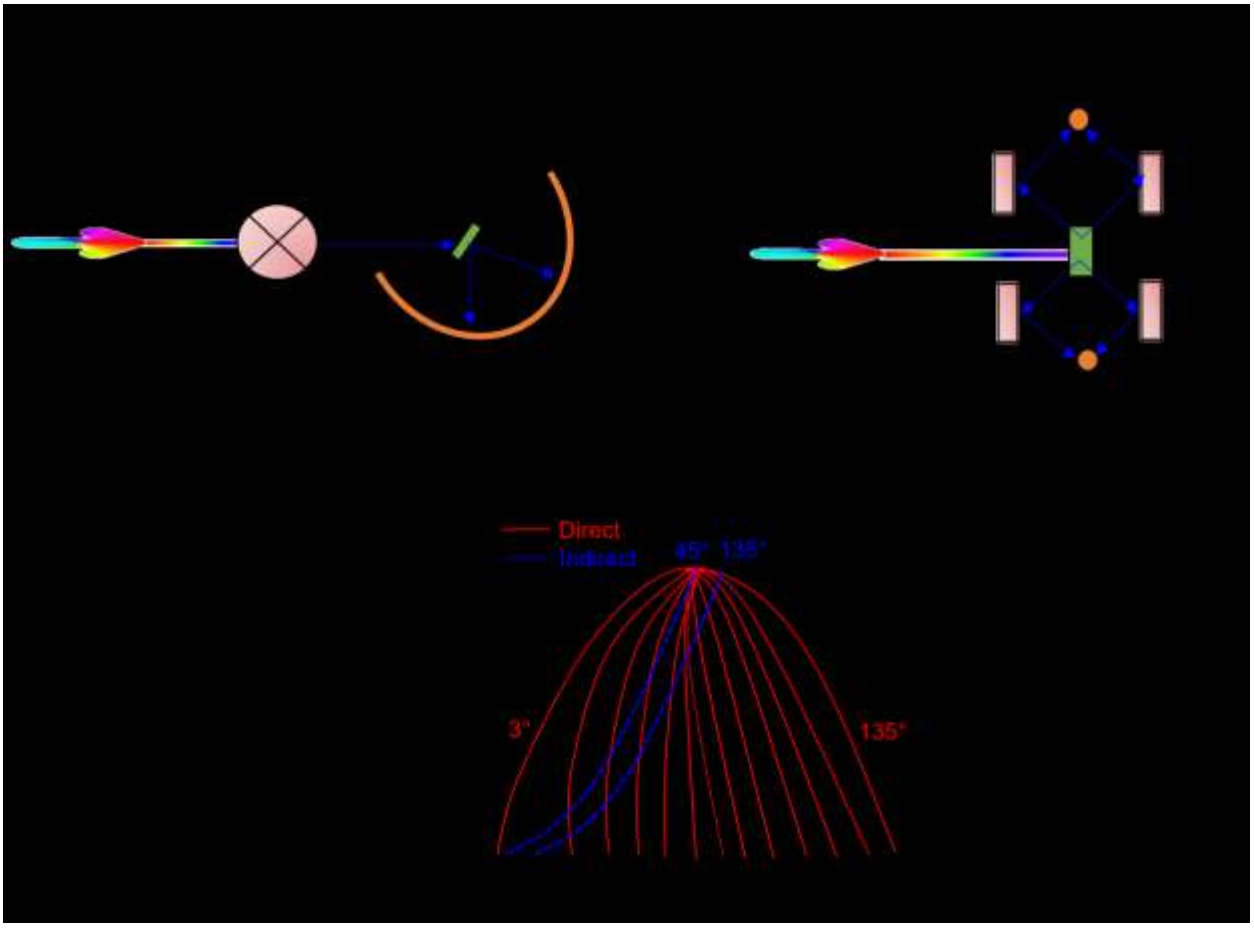

Scheme 1. (Top) Depiction of direct- (Left panel) and indirect-geometry (Right panel) instrumentation. (Bottom) Representation of trajectories in (Q, ω) space for a direct-geometry spectrometer with detectors at angles between 3° and 135° (red lines). Indirect-geometry spectrometer with scattering angles of 45° and 135°, forward scattering and backscattering, respectively (blue dashed lines).

The indirect-geometry INS spectrometers rely on a fixed E_f by crystals or filters while E_i is measured by time-of-flight of neutrons arriving on a small detector area (Scheme 1-Top right).[14] VISION, as an indirect-geometry instrument, offers two sets of analyzers/detectors corresponding to both forward (low $|\boldsymbol{Q}|$) and back (high $|\boldsymbol{Q}|$) scattering of neutrons.[12] E_f is usually specified to be small in energy (~28.2 cm^{-1} for

VISION). This technique gives energy transfer of 0-4000 cm^{-1} and Q ~2-13 $Å^{-1}$. The energy resolution of <1.5% $\Delta E/E$ is not determined by E_i as is the case with direct geometry instruments.[12, 15] While these instruments have good energy resolution, the exchange is a fixed trajectory through $\boldsymbol{Q}$ space.[14] For most energy transfers, E_i is much larger than E_f. Thus, the momentum transfer $\boldsymbol{Q}$ is almost equal to $\boldsymbol{k_i}$ irrespective of the scattering angle. Therefore, the $\boldsymbol{Q}$ value is dependent on E given by the relationship: $E = 16.7Q^2$.[14] VISION has two banks of analyzers with two different scattering angles, one at 45° (forward scattering) and another at 135° (backscattering) giving two spectra per experiment.

For the current work at VISION, samples of **1-d_4** and **1-d_{18}**, approximately 2 g each, were sealed in two aluminum containers and studied separately; **1-d_4** at 5, 50, 100 and 150 K; **1-d_{18}** at 5, 25, 50, 100 and 150 K. The INS data for **1-d_4** and **1-d_{18}** were measured for 1 h and 2 h, respectively, at each temperature.

Intra-Ground-State KD_1, "M_S = -1/2 (ϕ_1) → +1/2 (ϕ_2)" Transition in 1-d_{18} as Observed in INS

Without the application of the external field, the ground-state Kramers doublet KD_1 (Figure 1) in **1-d_{18}** is degenerate. On the application of the field, KD_1 is split by the Zeeman effect into the ground M_S = -1/2 (ϕ_1) and excited M_S = +1/2 (ϕ_2) states. We have studied the transitions between the M_S = -1/2 (ϕ_1) and M_S = +1/2 (ϕ_2) levels in a powder sample of **1-d_{18}** at 1.7 K with variable magnetic fields of 2.00(2) T, 4.00(4) T, 6.00(6) T, 8.00(8) T and 10.0(1) T using incident neutron energy of 32.6 cm^{-1}.

As shown in Figure 2, the transitions at the external magnetic field of 2.00(2) T is

observed at ca. 2.3(1.0) cm^{-1}. The transition broadens and shifts to higher energy with the increasing field up to 10.0(1) T. The *approximate* positions of the peaks vs. fields are summarized in Table 1, showing that the gap between the M_S = -1/2 (ϕ_1) and +1/2 (ϕ_2) states increases at ca. 1.1 cm^{-1}/T.

Table 1. Approximate positions of the intra-KD_1 transition in **1-d_{18}** vs external magnetic fields

Magnetic field (T)	2.00(2)	4.00(4)	6.00(6)	8.00(8)	10.0(1)
Energy (cm^{-1})	2.3(1.0)	4.5(1.0)	6.7(1.0)	9.0(1.0)	11.2(1.0)

Since a powder sample was used, the INS spectra are an average of the B_x, B_y and B_z directions of the powders. The Zeeman splittings of the B_x, B_y and B_z directions are different, contributing to the peak widths. At higher external magnetic fields, differences among the three orientation-dependent splittings increase, leading to the broadening spectra.

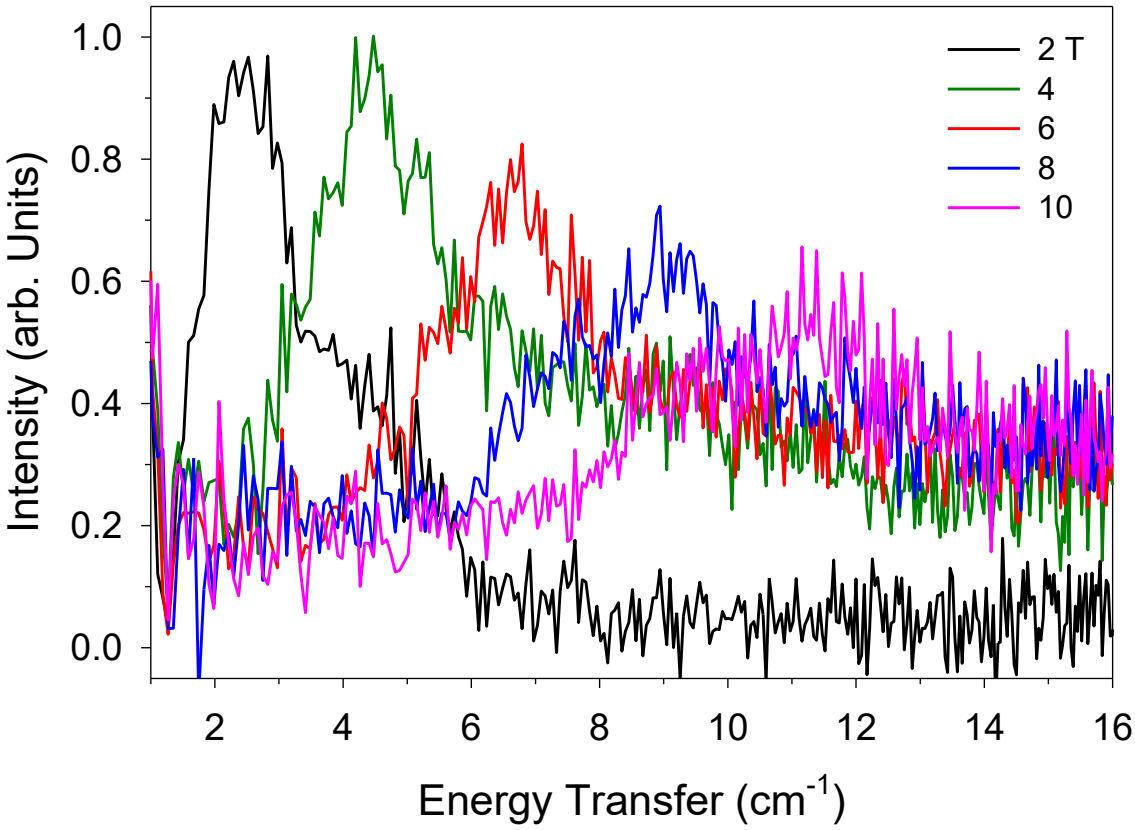

Figure 2. Variable-magnetic-field INS of **1-d_{18}** at DCS, revealing the "M_S = -1/2 (ϕ_1) → +1/2 (ϕ_2)" transition at 1.7 K. An alternative plot using binned data in the *x* axis (Energy Transfer) is given in Figure S2. Resolutions of the spectra are: (a) At Energy Transfer = 4 cm^{-1}, resolution = 1 cm^{-1}; (b) Energy Transfer = 12 cm^{-1}, resolution = 0.8 cm^{-1}.

To confirm the origin of the low energy transition due to magnetic scattering in Figure 2, the *Q*-dependence of the intra-ground-state Kramers doublet (KD_1) was studied. This data in Figure 3 show a decrease of the intensity as |***Q***| increases for the peak at 4.00(4) T, revealing its magnetic origin. A 2D plot of Energy Transfer vs. |***Q***| at 4.00(4) T and a comparison of the peak intensities at two different $|\boldsymbol{Q}|$ ranges are given in Figure S1 in Supporting Information.

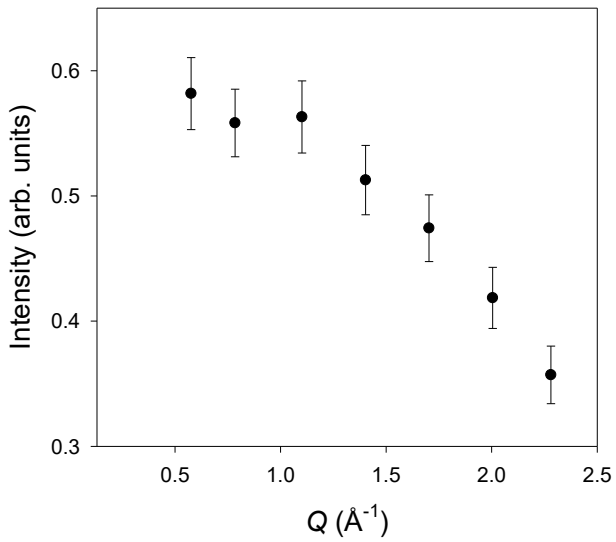

Figure 3. Change in intensity with ***Q*** of the intra-ground-state (KD_1) transition at 4.00(4) T (1.7 K).

The low-temperature, low-energy spectra in Figure 2 apparently reflect the angular dependence of the Zeeman splitting of the ground-state KD_1, as sketched in the inset of Figure 4. The appearance of this peak with the application of magnetic field confirms the sign of *D* is positive[7] and consistent with Figure 1c.

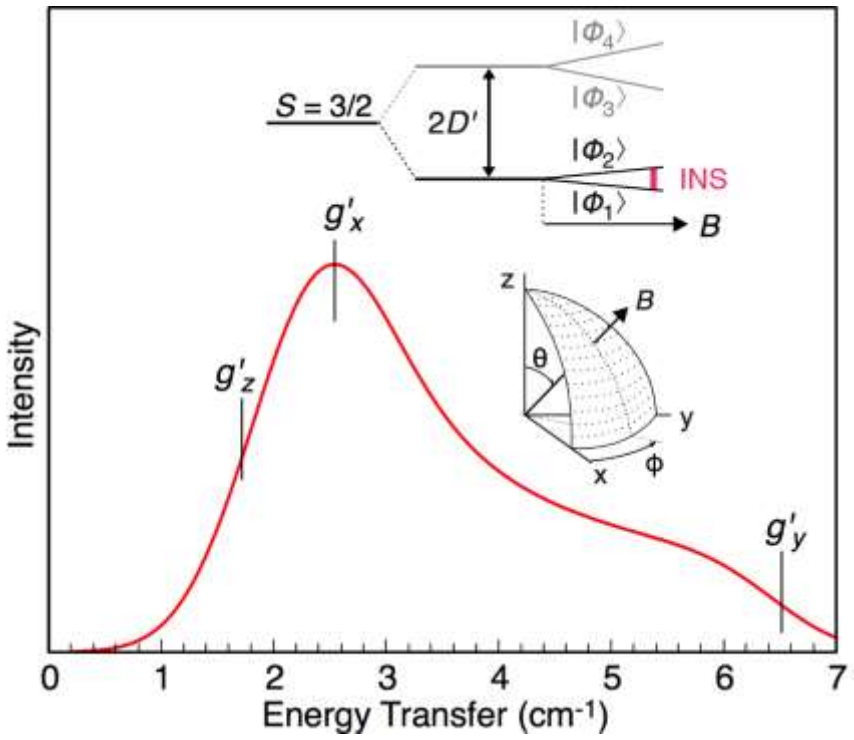

Figure 4. Spin-Hamiltonian simulation of the powder distribution of the INS transitions within the lowest Kramers doublet of the S = 3/2 system, arising from angular dependence of the Zeeman splitting for a field of 2 T at 1.7 K. Transition probabilities were obtained from the expression for Q = 0 Å^{-1} given in Eq. 2 (red line). The simulation is obtained with the parameters from the previous EPR and SQUID[7] analyses of **1** without any further fitting (Table 2, Gaussian lines, FWHM = 1 cm^{-1}). The black marks indicate the transitions with the field oriented along the principal axes of the effective spin g'-matrix, as obtained by EPR for the ground-state Kramers doublet (KD_1)[7] and reproduced by the spin-Hamiltonian.

The INS spectra were simulated by using the usual spin-Hamiltonian for S = 3/2 (Eq. 1) below:

$$\hat{H}_S = D\,[\hat{S}_z^2 - \frac{1}{3}S(S+1) + \frac{E}{D}(\hat{S}_x^2 - \hat{S}_y^2)] + \mu_B \vec{B}\cdot g \cdot \hat{\vec{S}} \qquad (1)$$

where D and E/D are the axial and rhombic zero-field splitting parameters, and g is the g matrix for the system spin S. The Schrödinger equation was solved in the usual basis of $|S,M_S\rangle$ functions and the transition moments for magnetic scattering of non-polarized neutrons by a powder sample according to the selection rules: $\Delta S = 0, \pm 1$ and $\Delta M_S = 0, \pm 1$ (approximated for $Q = 0$ Å^{-1}).[3g]

$$I_{INS}(Q=0) \propto \exp\left(\frac{-E_i}{kT}\right)\left(2\left|\langle\Psi_f|\hat{s}_z|\Psi_i\rangle\right|^2 + \left|\langle\Psi_f|\hat{s}_+|\Psi_i\rangle\right|^2 + \left|\langle\Psi_f|\hat{s}_-|\Psi_i\rangle\right|^2\right) \qquad (2)$$

We note that the spin-Hamiltonian and the parameters used [D, E/D and g (Table 2)] readily reproduce the effective g-values, g' ($g'_x = 2.65$, $g'_y = 6.95$, $g'_z = 1.83$), obtained previously from EPR (Ref. 7, best solution given in Supplementary Table 1 of the paper). Since ZFS of the spin quartet is very large, these observables (g') practically do not depend on fields up to 10.0(1) T. In other words, the KD_1-KD_2 inter-doublet mixing induced by the magnetic field is negligible, and alternatively the same simulation of INS spectra could be obtained for an isolated ground-state KD_1, described by effective spin $S' = 1/2$ and effective g'-values only (not shown).

The relatively good match of INS simulations and experimental spectra over a wide field range (Figure 5) indicates how, in principle, low-temperature INS spectra could be used for probing anisotropic effective spin 1/2 g'-values. The powder patterns

closely resemble those of corresponding EPR absorption spectra, obtained by numerical integration of the usually recorded derivative spectra (except that EPR spectra were recorded on a magnetic field axis and obey somewhat different selection rules). In both cases, the principal values of the anisotropic effective spin 1/2 *g′*-matrix can be estimated from the maximum of the absorption pattern and the inflection point of the wings of the powder distribution (tick marks in Figure 4). The assignment to magnetic axes, however, can be obtained from the spin-Hamiltonian interpretation.

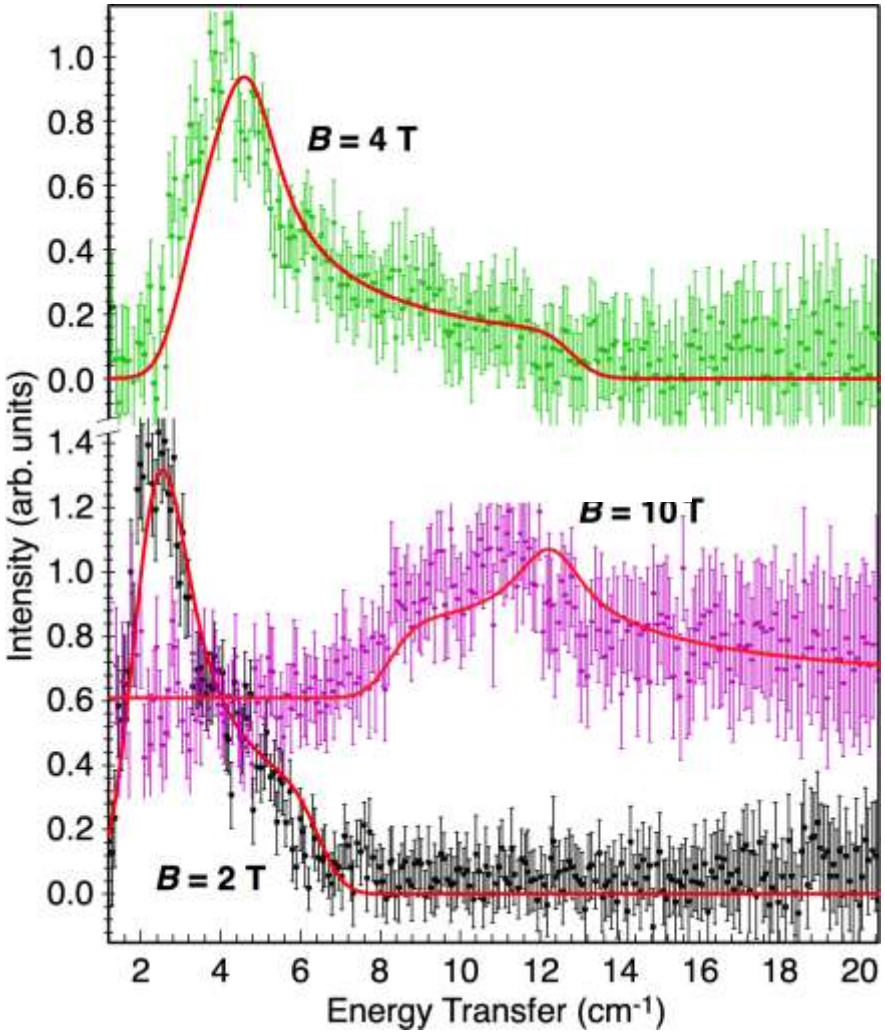

Figure 5. Comparison of the experimental and simulated INS spectra obtained at 1.7 K

with fields of 2.00(2), 4.00(4) and 10.0(1) T applied perpendicular to the incident neutron beam. In the figure, an offset of 0.6 units was added to the 10-T data for better overview. Error bars and values in parentheses indicate one standard deviation.

Table 2. Spin-Hamiltonian parameters from Ref. 7 used to simulate INS spectra [2.00(2), 4.00(4), 10.0(1) T data]

D	E/D	g_x, g_y, g_z
57 cm^{-1}	0.31	2.50, 2.57, 2.40

Inter KD, "M_S = ±1/2 ($\phi_{1,2}$) → ±3/2 ($\phi_{3,4}$)" Transition in 1-d_4 and 1-d_{18} Probed by INS

Previous Raman and far-IR work has demonstrated the presence of spin-phonon coupled peaks in **1-*d*$_4$** and **1-*d*$_{18}$**.[8a] Because the signal/noise ratio of DCS data prevents a conclusive assignment, we focus below on studying the transition "M_S = ±1/2 ($\phi_{1,2}$) → ±3/2 ($\phi_{3,4}$)" transition in **1-*d*$_4$** and **1-*d*$_{18}$** (Figure 1c) by INS at VISION without a magnet. The mostly spin (B) and phonon (A) peaks are present in the VT INS recorded at VISION (Figure 6). These peaks are initially overlapping at 5 K, B (115.4 cm^{-1} for **1-*d*$_4$** and 112.7 cm^{-1} for **1-*d*$_{18}$**) decreases in intensity with temperature increase, when the excited ZFS state is gradually populated, confirming its dominant magnetic origin. Phonon A is revealed at 150 K (**1-*d*$_4$**) and 25 and 50 K (**1-*d*$_{18}$**). The phonon on the right shoulder of B (~120 cm^{-1}) in **1-*d*$_4$** is an A_u mode.[8a] Most phonons in Figure 6 seem to soften, or decrease in energy, with increasing temperature. The softening is generally attributed to thermal expansion.[16] Reduction of the phonon intensity is expected because of the Debye-Waller factor, especially at high energy transfers (with relatively

high |***Q***| determined by the instrument geometry; Figures 7-8). We note that in **1-*d*$_4$** and **1-*d*$_{18}$**, the magnetic peaks are strong. Thus, it is straightforward to distinguish the temperature dependences between magnetic and phonon peaks. However, if the magnetic peak is weak and/or overlapping with a phonon, it would be very difficult to use this temperature-dependence method. Unlike far-IR[17] and Raman, external magnetic fields are not necessary to determine ZFS peaks in INS in this case.

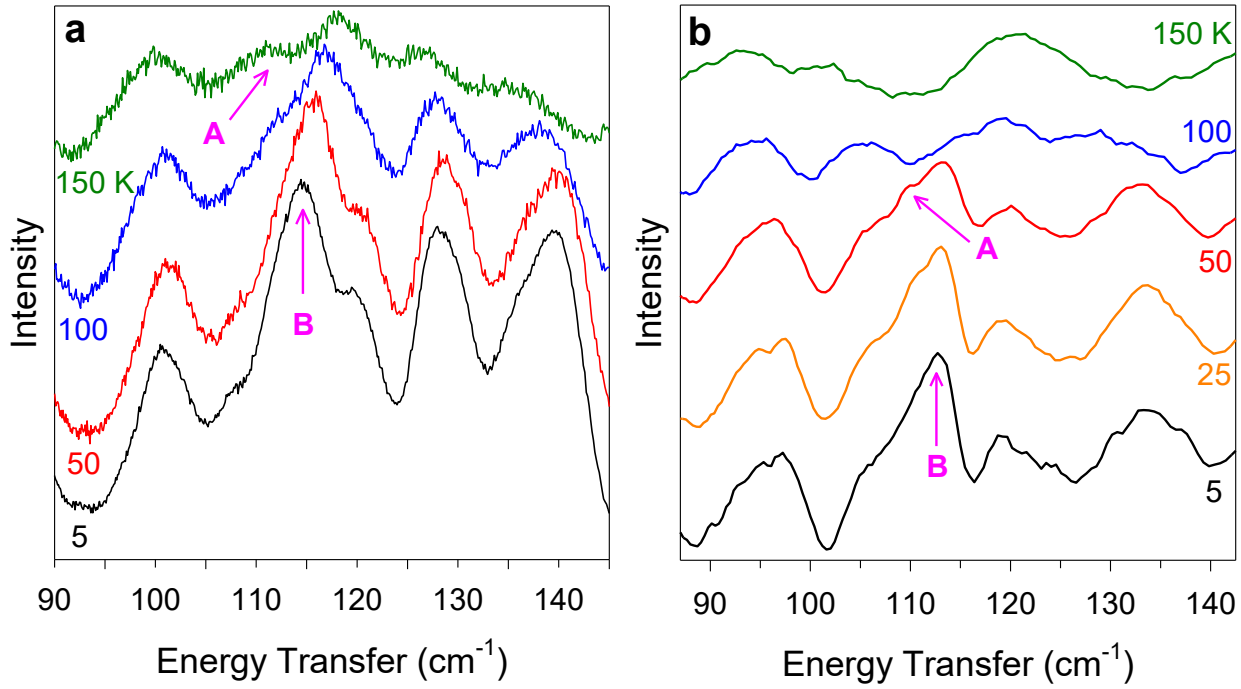

Figure 6. INS spectra at variable temperatures without external magnetic fields recorded at VISION: (a) **1-*d*$_4$**; (b) **1-*d*$_{18}$**. Peaks A and B are labelled.

Additional, Bose-corrected INS spectra of **1-*d*$_4$** and **1-*d*$_{18}$** are given in Figures 7 and 8, respectively. The Bose correction here is a numerical normalization of INS spectra measured at different temperatures.[2b],[14] The non-phonon modes, with different temperature dependence than the phonon modes, are not properly normalized and thus

behave differently. Thus, these non-phonon modes are highlighted and better recognized. One effect of the correction is that all spectra are brought to about the same baseline in order to see which peak behaves differently based on the Boltzmann statistics. From the Bose-corrected (both forward and back scattered) spectra of **1-*d*$_4$** and **1-*d*$_{18}$**, the overlapping peaks A and B near 114 cm^{-1} in the spectra of both **1-*d*$_4$** and **1-*d*$_{18}$** behave differently from other peaks. The overlapping peaks are identified to be the spin-phonon coupled peaks A and B, carrying magnetic features. Another observation is that, as expected, the phonon features of **1-*d*$_{18}$** are revealed better in the backscattering spectra in Figure 8b than in the forward scattering spectra Figure 8a.

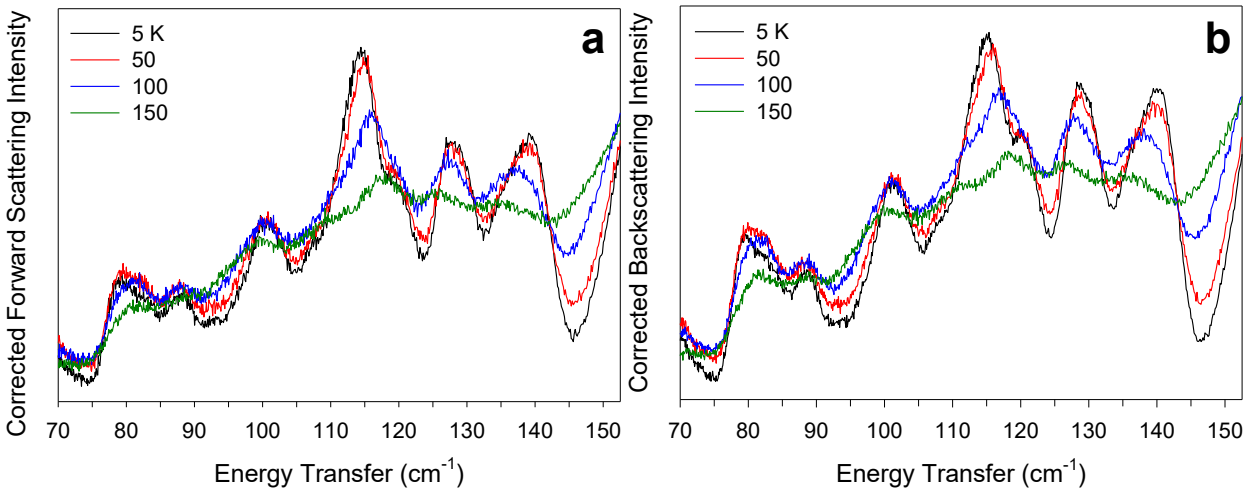

Figure 7. Bose-corrected INS spectra of **1-*d*$_4$** collected at VISION. (a) Forward scattering (low |***Q***|). (b) Backscattering (high |***Q***|).

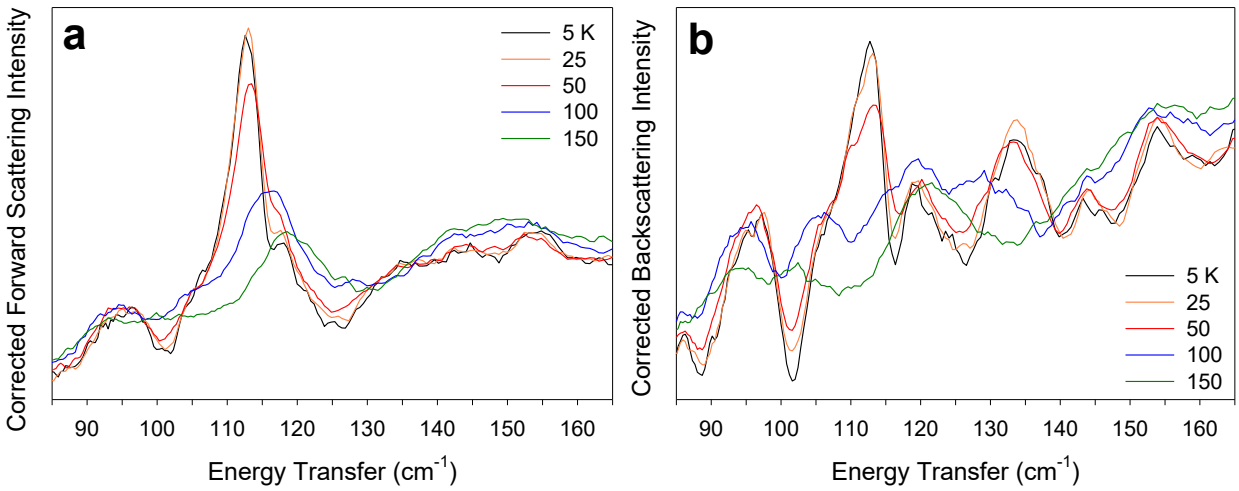

Figure 8. Bose-corrected INS spectra of **1-*d*$_{18}$** collected at VISION. (a) Forward scattering (low |***Q***|). (b) Backscattering (high |***Q***|).

Electrons and phonons are fermions and bosons, respectively. As shown earlier in the far-IR and Raman studies of **1-*d*$_4$** and **1-*d*$_{18}$**, spin-phonon coupling of peaks A and B makes both peaks to possess partial magnetic as well as phonon features.[8a] Such spin-phonon coupling at 0 T between peaks A and B is especially prominent in **1-*d*$_{18}$**.[8a] The coupling is expected to affect the Bose correction of peaks A and B, but it is not clear what the effect is. In other words, how should the spin-phonon modes be normalized to properly consider their own temperature dependence? To our knowledge, this issue has not been studied theoretically or experimentally, and it deserves a separate study.

The VT-INS spectra in the current work confirm the magnitude of the ZFS peak (114 cm^{-1}) previously probed by magnetometry and Raman and far-IR spectroscopies. Uniquely, the INS spectra here in Figures 6-8 exhibit both the magnetic and phonon features of the coupled peaks, while far-IR and Raman spectra demonstrate the

magnetic and phonon portions, respectively.[8a]

Non-magnetic $Zn(acac)_2(D_2O)_2$ (**2-*d*$_4$**) was studied at 5 K on VISION. A comparison of its INS spectrum with that of $Co(acac)_2(D_2O)_2$ (**1-*d*$_4$**) at 5 K and 150 K is given in Figure S5, supporting the assignment of the magnetic peak at ca. 114 cm^{-1} in **1-*d*$_4$** and the use of non-magnetic analog in assigning magnetic peak.

Periodic DFT Phonon Calculations and Comparison with INS Spectra

In molecular solids, modes in which the molecules vibrate primarily as a whole with little internal distortion, *i.e.*, lattice vibrations, are often characterized as external (intermolecular) modes, whereas significant distortions of atoms that comprise a part of the molecule with a small displacement of the molecular center-of-mass are often characterized as internal modes (intramolecular).[16] In other words, if the primary features of the mode involve significant distortions of atoms in the molecule, it is called an internal mode. The internal modes are also known as molecular vibrations, and they typically have much higher frequencies than the external modes. The external modes include translational and librational modes.[18] However, the internal and external modes often couple. In other words, all modes are essentially mixed. From the perspectives of solid-state physics, the internal and external modes originate from the same governing equations, and have the same mathematical representations.

For molecular crystal containing *n* atoms in *m* molecules per unit cell, there are 3*n*-6*m* internal modes and 6*m*-3 external modes, in addition to 3 acoustic modes.[16] Both internal and external modes as well as acoustic modes in molecular crystals are called phonons.[18] The internal and external modes are also named optical phonons.

Before comparing the periodic DFT phonon calculations with experiments, it is worth contrasting the features of phonons in INS with those in far-IR and Raman. As indicated earlier, INS is a unique technique to study phonons. Optical IR and Raman spectroscopies each have selection rules for phonon (vibrational) transitions. Some modes may be neither IR- nor Raman-active. INS, based on kinetic energy transfer between the incident neutrons and the sample, has no selection rules for phonons. In other words, all phonon modes are, in principle, active in INS.[14] This is an advantage compared with optical spectroscopies. In addition, peak intensities in INS and optical spectroscopies are different. Intensities of INS peaks are correlated to the atomic displacements of the atoms involved in scattering[14], whereas optical intensities stem from changes in the electronic properties of the atoms.[14] Therefore, for hydrogen-containing samples, incoherent scattering from H atoms tends to dominate their INS spectra. In contrast, optical techniques are affected by the atomic displacements of electron-rich atoms more so than electron-poor atoms. Deuteration significantly changes the INS spectra. With deuteration, modes that involve hydrogen scattering will shift in energy and appear weaker or disappear from the spectrum, as D atoms have much smaller neutron scattering cross section than H atoms. In optical IR and Raman spectra, the energies (peak positions) of phonons are also affected by deuteration.

As indicated earlier, results of periodic DFT phonon calculations for the 70-160 cm^{-1} region of **1-*d*$_4$** and **1-*d*$_{18}$**, including movies of the phonons 109.2 cm^{-1}, 126.0 cm^{-1}, 129.3 cm^{-1} and 142.7 cm^{-1} of **1-*d*$_4$**, and 116.3 cm^{-1} of **1-*d*$_{18}$**, have been presented in Ref. 8a (Supplementary Information) but have not been compared with INS spectra. In addition, INS spectra of the 15-250 cm^{-1} region at 5 and 100 K for **1-*d*$_4$** at VISION have

also been presented in Ref. 8b to show its methyl torsion peak. In the current work, the calculated phonons for the entire 0-4000 cm^{-1} region are given for comparison with the experimental INS spectra. INS spectra of **1-*d*$_4$** in the 15-250 cm^{-1} region at 5 and 100 K were given to understand the effect of magnetic fields on the methyl rotation in QENS spectra in Ref. 8b.

Full ranges of the calculated vs. the experimental INS spectra are given in Figures 9 and 10, although there are not many features over 1000 cm^{-1} (Figure 10). Two questions have been raised in analyzing the spectra: (a) How well do the calculated spectra match the experimental INS spectra? (b) How does the higher degree of deuteration in **1-*d*$_{18}$** affect the spectra, beyond the expected red shifts (to lower energies) of the phonon peaks by heavier D atoms?

Over all, the calculated vs. the experimental INS spectra match well, although the agreement is not perfect. The match between the calculated vs. the experimental INS spectra of **1-*d*$_4$** in Figures 9a and 10a seems to be better than that of **1-*d*$_{18}$** in Figures 9b and 10b. Following considerations may help answer the two questions. First, the low-energy region (in the current case below 250 cm^{-1}) comprises intermolecular phonon modes whose frequencies are very sensitive to the accuracy of the crystal structure model and the intermolecular interactions. Compared to intramolecular interactions such as covalent bonds, the intermolecular interactions in molecular systems are often difficult to calculate due to the lack of systematic and accurate methods to model van der Waals interactions. Thus, frequency calculation of these modes is well known to be challenging. Typically these modes involve translational, librational, or rotational motion of molecules (or subgroup of molecules such as methyl groups here), and have low

frequencies. Second, the reported crystal structure of nondeuterated **1** at 100 K[8a] was used in the calculations of phonons in **1-*d*$_4$** and **1-*d*$_{18}$**. H atoms were replaced by D atoms to calculate vibrational frequencies/modes using the mass of D atoms while keeping the structure unchanged. INS spectra were then calculated with the neutron cross-section of D atoms. Deuteration is known to affect intermolecular interactions and crystal structures by, e.g., mimicking the pressure effect by heavier D atoms.[19] Perdeuterated **1-*d*$_{18}$** is expected to experience more of the deuteration effects than **1-*d*$_4$**. However, such effects were not considered, as the corrections are beyond the current DFT model. Third, peaks in the INS spectra of **1-*d*$_{18}$** are often weaker because D atoms have a significantly smaller neutron scattering cross section than H atoms. The H atoms (in **1-*d*$_4$**) have much larger incoherent scattering (than the D atoms). However, in INS, the incoherent scattering does not mean high background or noise in the spectra. This is different from neutron diffraction. For the H-containing **1-*d*$_4$**, the strongest peaks are from the H atoms, and the peaks from the atomic displacements of Co, O, or C atoms are overwhelmed. When the sample is fully deuterated (as in **1-*d*$_{18}$**), peaks due to all elements show up better in its INS spectra. This is another effect of deuteration. If the DFT model reproduced the H-related peaks very well, but not so well for the Co-, O- or C-dominated peaks, the agreement between calculated and experimental INS spectra will be better for **1-*d*$_4$** (with more H atoms) than for **1-*d*$_{18}$**. Fourth, since the scattering from the **1-*d*$_{18}$** sample is significantly weaker, it is more susceptible to instrument background. Although known background has been subtracted, it is still possible that the spectrum contains unknown artifacts due to the much smaller signal/background ratio in the spectra of **1-*d*$_{18}$**.

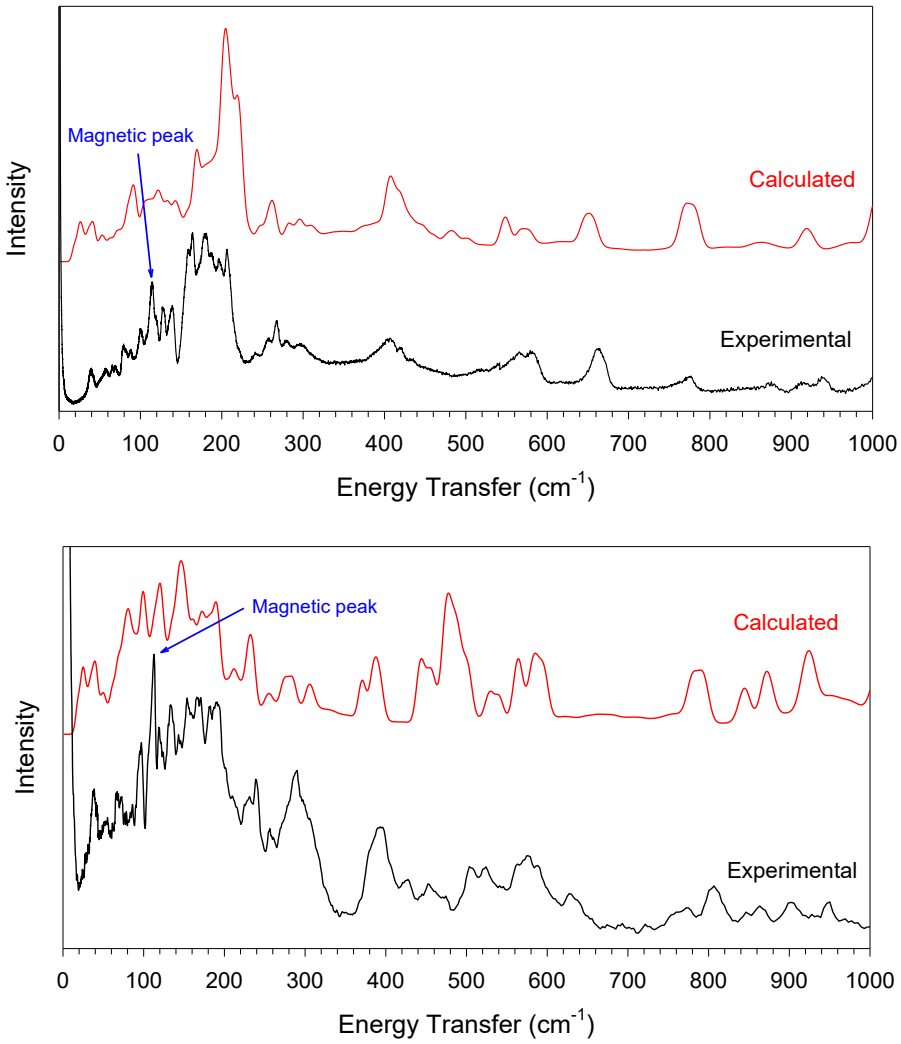

Figure 9. Calculated phonons and INS intensities (aCLIMAX) and experimental INS spectra from VISION at 5 K (backscattering data) in the 0-1000 cm^{-1} region: (Top) **1-*d*$_4$** and (Bottom) **1-*d*$_{18}$**.

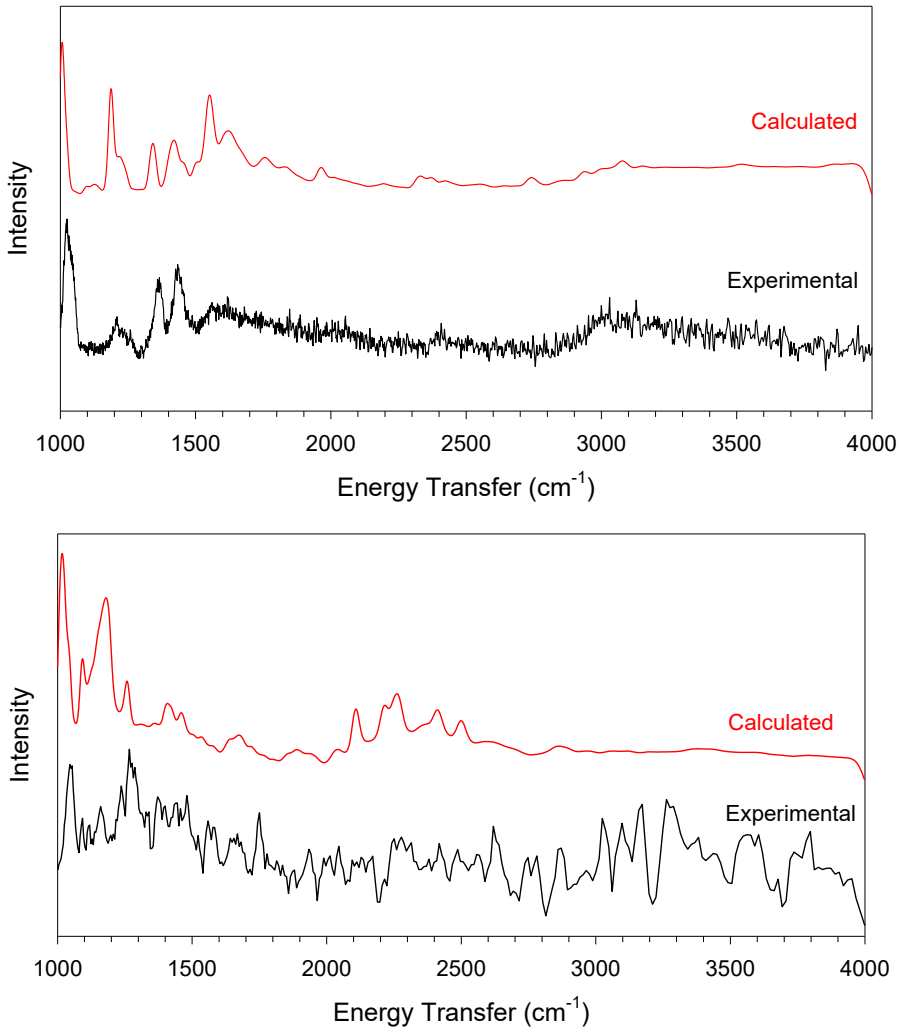

Figure 10. Calculated phonons and INS intensities (aCLIMAX) and experimental INS spectra at 5 K (backscattering data) from VISION in the 1000-4000 cm^{-1} region: (Top) **1-*d*$_4$** and (Bottom) **1-*d*$_{18}$**.

Conclusion

This work provides an example of using temperature-dependent INS to determine the magnetic and phonon peaks above >95 cm^{-1} for confirmation the magnitude of ZFS separation. Variable-field INS was also utilized to independently

determine the sign of the *D* parameter. In addition, the phonon calculations demonstrate the feasibility of accurately simulating phonons in molecular compounds to compare to the experimental INS spectra and to gain insights on the phonon environment around the ZFS peak. Indirect geometry spectrometers would be greatly enhanced by the ability to the coupled with an external magnetic field.

Experimental

Complexes **1-*d*$_4$** and **1-*d*$_{18}$** were prepared by the methods reported earlier.[8a] The synthesis of $Zn(acac)_2(D_2O)_2$ (**2-*d*$_4$**) and its X-ray powder diffraction pattern are given in Supporting Information.

In the variable-magnetic-field INS data at DCS,[11] the 10 T vertical magnet with a dilution refrigerator was used in the sample environment. Approximately 2 g of **1-*d*$_{18}$** were put on a piece of aluminum foil, rolled into a cigar shape, and then placed inside an aluminum sample holder. Data were measured at 1.7 K and 4.5 Å (32.6 cm^{-1}) for 0, 2, 4, 6, 8 and 10 T. In addition, the higher energy region was studied at 1.7 K and 1.8 Å (203.6 cm^{-1}) for 0 and 10 T. At DCS, a direct geometry instrument, data were collected up to 196 cm^{-1}. All data processing was completed with Data Analysis and Visualization Environment (DAVE).[20]

For VT INS at VISION, the samples, approximately 2 g, were sealed in an aluminum container. The INS spectra of **1-*d*$_4$** were measured at 5, 50, 100 and 150 K for 1 h at each temperature. **1-*d*$_{18}$** was measured at 5, 25, 50, 100 and 150 K for 2 h at each temperature. The phonon population effect was corrected by normalizing the INS intensity at energy transfer ω with $\coth\left(\frac{\hbar\omega}{2k_BT}\right)$.[14]

VASP[21] calculations were conducted and are described elsewhere.[8a] The aCLIMAX software[22] was used to convert the DFT calculated phonon results to the simulated INS spectra (Figures 9-10).

Author Contributions

S.E.S. and C.M.B. conducted the DCS experiments and interpreted the results. L.L.D. and Y.C. conducted the VISION experiments. S.E.S. and Y.C. interpreted the VISION results. A.J.R-C., Y.C. and S.E.S. conducted the phonon calculations. D.H.M. synthesized and characterized the complexes. E.B. simulated the EPR and susceptibility spectra with input from M.A. and F.N. Z-L.X. supervised the research. S.E.S., E.B., M.A. and Z-L.X. wrote the manuscript with input from other authors. All authors have given approval to the final version of the manuscript.

Notes

The authors declare no competing financial interest.

Acknowledgment

The authors thank financial support by the US National Science Foundation (CHE-1633870 to Z-L.X.), Deutsche Forschungsgemeinschaft (E.B., M.A., and F.N.), and a Shull Wollan Center Graduate Research Fellowship (S.E.S). Acknowledgment is also made to the Donors of the American Chemical Society Petroleum Research Fund for partial support of this work. The research at ORNL's Spallation Neutron Source was sponsored by the Scientific User Facilities Division, Office of Basic Energy Sciences,

U.S. Department of Energy. Computational resources for the VASP DFT and INS calculations were made available through the VirtuES and ICE-MAN projects, funded by the Laboratory Directed Research and Development at ORNL.

Keywords: cobalt · zero-field splitting · Inelastic Neutron Scattering · phonons · *ab initio* phonon calculations

References

[1] J. Krzystek and J. Telser, *Dalton Trans.* **2016**, *45*, 16751-16763.

[2] a) A. Furrer, J. Mesot and T. Strässle, *Neutron Scattering in Condensed Matter Physics*, World Scientific, **2009**; b) E. Colacio, J. Ruiz, E. Ruiz, E. Cremades, J. Krzystek, S. Carretta, J. Cano, T. Guidi, W. Wernsdorfer and E. K. Brechin, *Angew. Chem.* **2013**, *125*, 9300-9304. *Angew. Chem. Int. Ed.* **2013**, *52*, 9130-9134.

[3] a) D. Pinkowicz, H. I. Southerland, C. Avendaño, A. Prosvirin, C. Sanders, W. Wernsdorfer, K. S. Pedersen, J. Dreiser, R. Clérac, J. Nehrkorn, G. G. Simeoni, A. Schnegg, K. Holldack and K. R. Dunbar, **2015**, *137*, 14406-14422; b) J. Dreiser, A. Schnegg, K. Holldack, K. S. Pedersen, M. Schau‐Magnussen, J. Nehrkorn, P. Tregenna‐Piggott, H. Mutka, H. Weihe, J. Bendix and O. Waldmann, *Chem. Eur. J.* **2011**, *17*, 7492-7498; c) H. Andres, R. Basler, H.-U. Güdel, G. Aromí, G. Christou, H. Büttner and B. Rufflé, *J. Am. Chem. Soc.* **2000**, *122*, 12469-12477; d) R. Basler, A. Sieber, G. Chaboussant, H. U. Güdel, N. E. Chakov, M. Soler, G. Christou, A. Desmedt and R. Lechner, *Inorg. Chem.* **2005**, *44*, 649-653; e) Y.

Zhong, M. P. Sarachik, J. R. Friedman, R. A. Robinson, T. M. Kelley, H. Nakotte, A. C. Christianson, F. Trouw, S. M. J. Aubin and D. N. Hendrickson, *J. Appl. Phys.* **1999**, *85*, 5636-5638; f) I. Mirebeau, M. Hennion, H. Casalta, H. Andres, H. U. Güdel, A. V. Irodova and A. Caneschi, *Phys. Rev. Lett.* **1999**, *83*, 628-631; g) R. Basler, P. L. W. Tregenna-Piggott, H. Andres, C. Dobe, H.-U. Güdel, S. Janssen and G. J. McIntyre, *J. Am. Chem. Soc.* **2001**, *123*, 3377-3378; h) L. Chen, H.-H. Cui, S. E. Stavretis, S. C. Hunter, Y.-Q. Zhang, X.-T. Chen, Y.-C. Sun, Z. Wang, Y. Song, A. A. Podlesnyak, Z.-W. Ouyang and Z.-L. Xue, *Inorg. Chem.* **2016**, *55*, 12603-12617; i) A. Sieber, C. Boskovic, R. Bircher, O. Waldmann, S. T. Ochsenbein, G. Chaboussant, H. U. Güdel, N. Kirchner, J. van Slageren, W. Wernsdorfer, A. Neels, H. Stoeckli-Evans, S. Janssen, F. Juranyi and H. Mutka, *Inorg. Chem.* **2005**, *44*, 4315-4325; j) M. Sigrist, P. L. W. Tregenna-Piggott, K. S. Pedersen, M. A. Sørensen, A.-L. Barra, J. Hauser, S.-X. Liu, S. Decurtins, H. Mutka and J. Bendix, *Eur. J. Inorg. Chem.* **2015**, *2015*, 2683-2689; k) R. Bircher, G. Chaboussant, S. T. Ochsenbein, F. Fernandez-Alonso, H. U. Güdel and E. K. Brechin, *Polyhedron* **2005**, *24*, 2455-2458; l) S. Ansbro, E. Moreno-Pineda, W. Yu, J. Ollivier, H. Mutka, M. Ruben and A. Chiesa, *Dalton Trans.* **2018**, *47*, 11953-11959; m) S. E. Stavretis, M. Atanasov, A. A. Podlesnyak, S. C. Hunter, F. Neese and Z.-L. Xue, *Inorg. Chem.* **2015**, *54*, 9790-9801; n) S. C. Hunter, A. A. Podlesnyak and Z.-L. Xue, *Inorg. Chem.* **2014**, *53*, 1955-1961.

[4] a) M. J. Giansiracusa, M. Vonci, W. Van den Heuvel, R. W. Gable, B. Moubaraki, K. S. Murray, D. Yu, R. A. Mole, A. Soncini and C. Boskovic, *Inorg. Chem.* **2016**, *55*, 5201-5214; b) M. Kofu, O. Yamamuro, T. Kajiwara, Y. Yoshimura, M. Nakano,

K. Nakajima, S. Ohira-Kawamura, T. Kikuchi and Y. Inamura, *Phys. Rev. B* **2013**, *88*, 064405; c) M. Vonci, M. J. Giansiracusa, W. Van den Heuvel, R. W. Gable, B. Moubaraki, K. S. Murray, D. Yu, R. A. Mole, A. Soncini and C. Boskovic, *Inorg. Chem.* **2017**, *56*, 378-394; d) K. S. Pedersen, L. Ungur, M. Sigrist, A. Sundt, M. Schau-Magnussen, V. Vieru, H. Mutka, S. Rols, H. Weihe, O. Waldmann, L. F. Chibotaru, J. Bendix and J. Dreiser, *Chem. Sci.* **2014**, *5*, 1650-1660; e) K. Prša, J. Nehrkorn, J. Corbey, W. Evans, S. Demir, J. Long, T. Guidi and O. Waldmann, *Magnetochemistry* **2016**, *2*, 45; f) R. Marx, F. Moro, M. Dorfel, L. Ungur, M. Waters, S. D. Jiang, M. Orlita, J. Taylor, W. Frey, L. F. Chibotaru and J. van Slageren, *Chem. Sci.* **2014**, *5*, 3287-3293; g) M. L. Baker, T. Tanaka, R. Murakami, S. Ohira-Kawamura, K. Nakajima, T. Ishida and H. Nojiri, *Inorg. Chem.* **2015**, *54*, 5732-5738; h) M. A. Sørensen, U. B. Hansen, M. Perfetti, K. S. Pedersen, E. Bartolomé, G. G. Simeoni, H. Mutka, S. Rols, M. Jeong, I. Zivkovic, M. Retuerto, A. Arauzo, J. Bartolomé, S. Piligkos, H. Weihe, L. H. Doerrer, J. van Slageren, H. M. Rønnow, K. Lefmann and J. Bendix, *Nat. Commun.* **2018**, *9*, 1292; i) M. Perfetti, M. A. Sørensen, U. B. Hansen, H. Bamberger, S. Lenz, P. P. Hallmen, T. Fennell, G. G. Simeoni, A. Arauzo, J. Bartolomé, E. Bartolomé, K. Lefmann, H. Weihe, J. van Slageren and J. Bendix, *Adv. Funct. Mater.* **2018**, *28*, 1801846; j) M. J. Giansiracusa, E. Moreno-Pineda, R. Hussain, R. Marx, M. Martínez Prada, P. Neugebauer, S. Al-Badran, D. Collison, F. Tuna, J. van Slageren, S. Carretta, T. Guidi, E. J. L. McInnes, R. E. P. Winpenny and N. F. Chilton, *J. Am. Chem. Soc.* **2018**, *140*, 2504-2513.

[5] a) J. M. Frost, K. L. M. Harriman and M. Murugesu, *Chem. Sci.* **2016**, *7*, 2470-2491; b) S. T. Liddle and J. van Slageren, *Chem. Soc. Rev.* **2015**, *44*, 6655-6669.

[6] B. S. Hudson in *Vibrational Spectroscopy via Inelastic Neutron Scattering*, (Ed. J. Laane), Elsevier, Amsterdam, **2009**, pp. 597-622.

[7] S. Gómez-Coca, A. Urtizberea, E. Cremades, P. J. Alonso, A. Camón, E. Ruiz and F. Luis, *Nat. Commun.* **2014**, *5*, 4300.

[8] a) D. H. Moseley, S. E. Stavretis, K. Thirunavukkuarasu, M. Ozerov, Y. Cheng, L. L. Daemen, J. Ludwig, Z. Lu, D. Smirnov, C. M. Brown, M. Atanasov, E. Bill, F. Neese, A. Pandey, A. J. Ramirez-Cuesta, A. C. Lamb and Z.-L. Xue, *Nat. Commun.* **2018**, *9*, 2572; b) S. E. Stavretis, E. Mamontov, D. H. Moseley, Y. Cheng, L. L. Daemen, A. J. Ramirez-Cuesta and Z.-L. Xue, *Phys. Chem. Chem. Phys.* **2018**, *20*, 21119-21126.

[9] J. R. Pilbrow, *J. Magn. Reson.* **1978**, *31*, 479-490.

[10] a) O. Waldmann, G. Carver, C. Dobe, A. Sieber, H. U. Güdel and H. Mutka, *J. Am. Chem. Soc.* **2007**, *129*, 1526-1527; b) K. Ridier, S. Petit, B. Gillon, G. Chaboussant, D. A. Safin and Y. Garcia, *Phys. Rev. B* **2014**, *90*, 104407.

[11] J. R. D. Copley and J. C. Cook, *Chem. Phys.* **2003**, *292*, 477-485.

[12] P. A. Seeger, L. L. Daemen and J. Z. Larese, *Nucl. Instr. Meth. Phys. Res. A* **2009**, *604*, 719-728.

[13] R. Eccleston in *Time-of-Flight Inelastic Scattering in Neutron and X-ray Spectroscopy*, Eds.: F. Hippert, E. Geissler, J. L. Hodeau, E. Lelièvre-Berna and J.-R. Regnard), Springer, Dordrecht, **2006**, pp. 457-482.

[14] P. C. H. Mitchell, S. F. Parker, A. J. Ramirez-Cuesta and J. Tomkinson, *Vibrational Spectroscopy with Neutrons: With Applications in Chemistry, Biology, Materials Science and Catalysis*, World Scientific Publishing Company, **2005**, pp. 552-558.

[15] S. F. Parker, A. J. Ramirez-Cuesta and L. Daemen, *Spectrochim. Acta A* **2018**, *190*, 518-523.

[16] M. T. Dove, *Introduction to Lattice Dynamics*, Cambridge University Press, **1993**.

[17] Y. Rechkemmer, F. D. Breitgoff, M. van der Meer, M. Atanasov, M. Hakl, M. Orlita, P. Neugebauer, F. Neese, B. Sarkar and J. van Slageren, *Nat. Commun.* **2016**, *7*, 10467.

[18] P. C. H. Mitchell, S. F. Parker, A. J. Ramirez-Cuesta and J. Tomkinson, *Vibrational Spectroscopy with Neutrons: With Applications in Chemistry, Biology, Materials Science and Catalysis*, World Scientific Publishing Company, **2005**.

[19] D. Wade, *Chem.-Biol. Interact.* **1999**, *117*, 191-217.

[20] R. T. Azuah, L. R. Kneller, Y. Qiu, P. L. W. Tregenna-Piggott, C. M. Brown, J. R. D. Copley and R. M. Dimeo, *J. Res. Natl. Inst. Stan. Technol.* **2009**, *114*, 341-358.

[21] G. Kresse and J. Furthmüller, *Phys. Rev. B* **1996**, *54*, 11169-11186.

[22] A. J. Ramirez-Cuesta, *Comput. Phys. Comm.* **2004**, *157*, 226-238.